Available online at www.sciencedirect.com
SCIENCE DIRECT®
International Journal of Multiphase Flow 32 (2006) 864–885
International Journal of Multiphase Flow
www.elsevier.com/locate/ijmulflow

Eulerian–Lagrangian simulations of unsteady gas–liquid flows in bubble columns

Vivek V. Buwa [1], Dhanannjay S. Deo [2], Vivek V. Ranade *

Industrial Flow Modelling Group, National Chemical Laboratory, Pune 411 008, India

Received 5 September 2004; received in revised form 15 March 2006

Abstract

We studied the dynamics of gas–liquid flows in a rectangular bubble column using Eulerian–Lagrangian simulations. Three-dimensional, unsteady simulations were performed to simulate the dynamic characteristics of the oscillating bubble plume. The effect of superficial gas velocity and aerated liquid height-to-column width (H/W) ratio on the dynamic and time-averaged flow properties was studied and the simulated results were validated using wall pressure and voidage fluctuation measurements. The effect of lift force and numerical diffusion on the dynamic and time-averaged properties is discussed in detail. Further, the results obtained using the Eulerian–Lagrangian simulations were compared with the Eulerian–Eulerian simulations. The bubble scale information, which is otherwise lost in the Eulerian–Eulerian simulations, was validated using the voidage fluctuation measurements. Such experimentally validated Eulerian–Lagrangian models will be useful for the simulation of mass transfer and reactions in bubble columns.

Keywords: Bubble column; Gas–liquid flow; Dynamics; Eulerian–Lagrangian simulations; Eulerian–Eulerian simulations; CFD

1. Introduction

Dispersed gas–liquid flows are encountered in a variety of applications (for example, gas–liquid reactions and mass and heat transfer operations). Dispersed gas–liquid flow in bubble columns is inherently unsteady and comprised of various flow processes occurring at different length and time scales. On the one hand, meandering bubble swarms give origin to macroscopic re-circulatory flow comprised of several ascending and descending vortical structures with length scales of the order of the column width or diameter and frequencies of the order of 0.1–1 Hz. On the other hand, bubble-scale flow (vortices shed by bubbles, flow around

* Corresponding author. Tel.: +91 20 2589 3400x2170; fax: +91 20 2589 3260.
E-mail addresses: vivek.buwa@lstm.uni-erlangen.de (V.V. Buwa), dsdeo@cpdm.iisc.ernet.in (D.S. Deo), vv.ranade@ncl.res.in (V.V. Ranade).
[1] Presently working at the Institute of Fluid Mechanics (LSTM), University of Erlangen—Nuremberg, Cauerstrasse 4, D-91058 Erlangen, Germany.
[2] Presently working at the Centre for Product Design and Manufacturing, Indian Institute of Science, Bangalore 560 012, India.

0301-9322/$ - see front matter © 2006 Elsevier Ltd. All rights reserved.
doi:10.1016/j.ijmultiphaseflow.2006.02.017

individual bubbles, bubble–bubble interactions) has length scales of the order of the bubble diameter and frequencies of the order of 1–10 Hz. The fluid turbulence has very different characteristic length and time scales. The overall dynamics is the result of interactions of these flow processes and govern mixing and other transport processes in bubble columns. It is therefore important to develop computational models capable of predicting quantitative relationship between unsteady fluid dynamics and various design/operating parameters.

Dispersed gas–liquid flows in bubble columns can be simulated using Eulerian–Eulerian and Eulerian–Lagrangian approaches. In the Eulerian–Eulerian (E–E) approach, each fluid phase is considered as a continuum in the domain under consideration which can interpenetrate with the other fluid phases. Several averaging methods (such as volume, time or ensemble averaging) are used to formulate basic governing equations. If the underlying flow is turbulent, appropriate turbulence models (generally the two-equation k–ε model) are used. In the Eulerian–Lagrangian (E–L) approach, the continuous phase is treated in an Eulerian framework (using averaged equations) whereas the motion of individual or groups of bubbles is simulated by solving the force balance on that bubble. The trajectories of several bubbles or groups are computed in the control volume and averaged at the computational level. In the Eulerian–Eulerian approach, the trajectory construction and subsequent averaging are not carried out explicitly during the computations. Since these operations are implicitly carried out at the conceptual level while deriving the equations, this approach requires less computational effort than the Eulerian–Lagrangian approach. However, the discrete character of the underlying process is lost in the Eulerian–Eulerian approach. The Eulerian–Lagrangian approach offers the following advantages at the cost of increased computational efforts:

- The bubble size distribution can be accounted in a simple manner which allows a more accurate description of inter-phase forces (drag, lift, virtual mass and other forces).
- Bubble–bubble interactions (four-way momentum exchange, bubble coalescence and break-up) and bubble-induced turbulence can be accounted for in a realistic way.
- Various transport processes and reactions occurring around and within individual bubbles can be rigorously modeled.

In previous numerical studies, unsteady gas–liquid flows in bubble columns were simulated using the Eulerian–Eulerian approach. It was observed that the Eulerian–Eulerian simulations can predict the low-frequency oscillations of the meandering bubble plume and time-averaged flow properties in reasonably good agreement with experiments (see, for example, Pfleger et al., 1999; Buwa and Ranade, 2002, 2003; Rampure et al., 2003, and references cited therein). Several attempts have also been made to simulate dispersed gas–liquid flows using the Eulerian–Lagrangian approach (see, for example, Delnoij et al., 1997a,b, 1999; Lain et al., 1999, 2002). Although the models based on the Eulerian–Lagrangian approach could predict well the time-averaged properties (such as gas and liquid velocity and their fluctuations), the ability of these models to predict dynamic characteristics and the bubble scale information is not yet established. In the present work, therefore, we studied the dynamics of gas–liquid flows using Eulerian–Lagrangian simulations in a rectangular bubble column the same one as that used previously for Eulerian–Eulerian simulations (Buwa and Ranade, 2003). Over the last several years, various issues regarding the modeling of dispersed gas–liquid flows using the Eulerian–Lagrangian approach have been investigated. These issues include various forces acting on bubbles and their magnitudes, inter-phase coupling between the continuous and dispersed phases (two- and four-way), prediction of bubble trajectories in turbulent flow and turbulence modulation by the presence of bubbles. A brief review of previous work in the light of these issues is presented in the following section.

1.1. Previous work

The important contributions relevant to the present work are summarized in Table 1. Lapin and Lubbert (1994) simulated unsteady gas–liquid flows in rectangular bubble columns. They simulated the motion of bubble clusters by assuming that the clusters have a fixed slip velocity. The momentum exchange between the gas and liquid phases was not considered. The coupling between the gas and liquid phases was achieved through the effective density of the mixture. The flow was assumed to be laminar. Using their model, they could

Table 1
Simulations of gas–liquid flow in bubble columns using the Eulerian–Lagrangian approach

Reference	Geometry	Momentum exchange	2-D/3-D	Turbulence model	Sparger details	Aspects investigated	Experimental validation
Lapin and Lubbert (1994)	1×4 m 0.5×1 m 1×1.5 m	Fixed slip velocity for bubble cluster	2-D	Laminar	Locally/uniformly aerated	Unsteady nature of gas–liquid flow in bubble column	–
Sokolichin et al. (1997)	Rectangular column as used by Becker et al. (1994)	Fixed slip velocity for bubble cluster	2-D	k–ε	Locally aerated	Effect of numerical diffusion (discretization scheme), comparison with Eulerian–Eulerian simulations	LDA measurement of Becker et al. (1994)
Delnoij et al. (1997a)	Rectangular column as used by Becker et al. (1994)	D, VM, L, hydro, bubble–bubble interaction	2-D	Laminar	Locally aerated	Effect of virtual mass, lift and hydrodynamic forces	LDA measurement of Becker et al. (1994)
Delnoij et al. (1997b)	Rectangular column • Width: 0.175 m Depth: 0.175 m H/W: 1–11.4 • $0.25 \times 2.0 \times 0.2$ m	D, VM, L	2-D	Laminar	Locally aerated	Effect of aspect ratio, superficial gas velocity	Plume oscillation period measured by videography
Delnoij et al. (1999)	Rectangular column • Width: 0.175 m Depth: 0.175 m H/W: 1–7.7	D, VM, L	3-D	Laminar	Locally aerated	Effect of dimensionality, aspect ratio, effect of momentum transfer due to bubble–bubble collisions	–
Lain et al. (1999)	Cylindrical column 0.14 m $D \times 6.5$ m H	D, VM, L	2-D	k–ε, bubble-induced turbulence	Uniformly aerated	Effect of bubble-induced turbulence	Time-averaged and fluctuating bubble rise velocity
Lain et al. (2002)	Cylindrical column 0.14 m $D \times 6.5$ m H	D, VM, L	2-D	k–ε, bubble-induced turbulence	Uniformly aerated	Effect of momentum and turbulence source due to bubbles	Time-averaged and fluctuating bubble rise velocity
Present work	Rectangular column • Width: 0.2 m Depth: 0.05 m H/W: 2.25, 4.5	D, VM, L	3-D	k–ε	Locally aerated	Effect of superficial gas velocity, H/W ratio, lift force, numerical diffusion on dynamic and time-averaged flow properties	Wall pressure and voidage fluctuation measurement of Buwa and Ranade (2002, 2005)

D: drag force, VM: virtual mass force, L: lift force, Hydro: hydrodynamic force, k–ε: standard k–ε model.

simulate the recirculatory flow generated by a locally/uniformly aerated sparger. Later, the same group used these simulations to assess the effect of numerical diffusion associated with Eulerian–Eulerian simulations (Sokolichin et al., 1997).

Delnoij et al. (1997a,b, 1999) simulated unsteady gas–liquid flow in a rectangular bubble column using the Eulerian–Lagrangian approach. The motion of bubbles was simulated by considering various forces acting on them, viz., pressure and gravity force, drag, lift, virtual mass and other hydrodynamic forces. They also developed a discrete bubble–bubble collision model to account for momentum exchange due to bubble collisions (four-way coupling). Delnoij et al. (1997a) studied the effect of lift force on the instantaneous and time-averaged flow properties. The inclusion of lift force with a lift coefficient of 0.53 led to a higher lateral dispersion of bubbles in the upper part of the column. Such lateral dispersion resulted in breakdown of the recirculatory flow in the upper part of the column. Since the momentum exchange due to bubble–bubble collision was found to be small compared with the momentum exchange due to various forces acting on the bubbles, in their 1999 study, they might not have considered the bubble–bubble collision model. Delnoij et al. (1997b) further used their model to study the effects of aspect ratio and superficial gas velocity on the motion of an oscillating bubble plume in a rectangular bubble column. Although they could capture the oscillatory behavior of the bubble plume, the predicted plume oscillation periods were 1.5–2 times higher than those observed experimentally. It should also be noted that in all their simulations the liquid phase flow was assumed to be laminar.

Lain et al. (1999, 2002) carried out two-dimensional simulations of gas–liquid flows in cylindrical bubble columns. They simulated the turbulent gas–liquid flow using the standard k–ε model. The coupling between the fluid phases was achieved through momentum source terms and source terms in the k and ε equations. Their results indicate that adequate modeling of bubble-induced turbulence source terms in the k and ε equations is necessary for accurate prediction of time-averaged liquid and bubble velocities and their fluctuations.

It should be noted that most of the simulation studies reported in the literature were carried out using two-dimensional geometry, the liquid phase was assumed to be laminar and the simulated results were in qualitative agreement with the experiments. Although the predicted time-averaged properties such as liquid and bubble velocity agreed well with the measurements, the predicted dynamic characteristics were not well studied and validated. For any progress in the development of these models, the simulated results on time-averaged fluid (gas and liquid) velocities and phase hold-ups together with simulated dynamic characteristics need to be compared with the experiments. The present work is carried out with this motivation.

1.2. Present work

We simulated unsteady gas–liquid flows in a rectangular bubble column. The geometry of the column was the same as that used for Eulerian–Eulerian simulations by Buwa and Ranade (2003). The force balance over individual bubbles was solved by considering pressure, buoyancy, gravity, lift and virtual mass forces. Three-dimensional, unsteady simulations were carried out to study the effects of superficial gas velocity and aerated liquid height (H) to column width (W) ratio. The effects of lift force and numerical diffusion on the dynamic and time-averaged properties were also studied. The simulated dynamic characteristics and time-averaged flow properties were compared with the voidage fluctuation measurements of Buwa and Ranade (2005). The results obtained using the Eulerian–Lagrangian simulations were compared with those obtained with the Eulerian–Eulerian simulations of Buwa and Ranade (2003). The additional bubble-scale information was validated using experimental measurements.

2. Experiments

A rectangular bubble column of 0.2 m width × 1.2 m height × 0.05 m depth was used (Fig. 1). This geometry was same as that used by Pfleger et al. (1999). All experiments were carried out using air as a sparged gas and tap water as a liquid phase, unless mentioned otherwise. The superficial air velocity was varied from 0.16 to 12.0 cm/s. A sparger with eight holes located at the center of the bottom cross-section (hole diameter

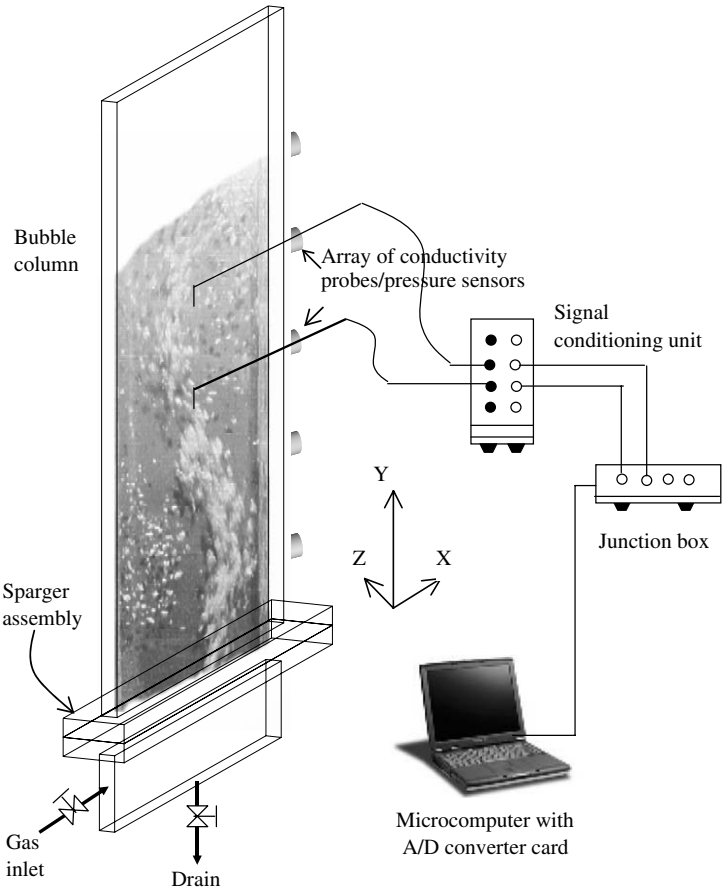

Fig. 1. Experimental set-up for characterization of gas–liquid flows in a rectangular bubble column.

0.8 mm, arranged in a square pitch of 6 mm) was used (see Buwa and Ranade, 2002, 2005 for more details of the experimental set-up and procedure).

In our earlier work, we characterized gas–liquid flows in the above-mentioned rectangular bubble columns using wall pressure and voidage fluctuations. Buwa and Ranade (2002) carried out wall pressure fluctuation measurements to characterize the low-frequency oscillations in rectangular bubble columns. They discussed the acquisition of wall pressure fluctuations and its analysis in detail and measured the plume oscillation period (time required for one oscillation of the bubble plume) for different superficial gas velocities, sparger configurations and H/W ratio. Pfleger et al. (1999) measured the time-averaged liquid velocity at different liquid heights for the same column geometry. In order to complement this dataset, Buwa and Ranade (2005) measured the time-averaged gas hold-up distribution and bubble passage frequencies at different H/W ratios using conductivity probes. In the present work, these measurements were used for validation of the numerical simulations.

3. Computational model

3.1. Governing equations

The mass conservation equation for the liquid phase (after Reynolds averaging) can be written as

$$\frac{\partial}{\partial t}(\rho_l \alpha_l) + \frac{\partial}{\partial x_j}(\rho_l \alpha_l U_{li}) = S_l \tag{1}$$

where ρ_l is the liquid density, α_l is the liquid volume fraction. The subscript S_l represents the source to liquid phase due to gas–liquid mass transfer and U_l is the mean liquid velocity. In the present work, gas–liquid mass transfer was not considered and therefore S_l was set to zero. The liquid-phase momentum conservation equation can be written as

$$\frac{\partial}{\partial t}(\rho_l \alpha_l U_{li}) + \frac{\partial}{\partial x_j}(\rho_l \alpha_l U_{li} U_{lj}) = -\alpha_l \frac{\partial P}{\partial x_i} + \frac{\partial}{\partial x_j}\left[\alpha_l \mu_{\mathrm{eff},l}\left(\frac{\partial U_{li}}{\partial x_j} + \frac{\partial U_{lj}}{\partial x_i}\right)\right] - \frac{2}{3}\frac{\partial}{\partial x_i}\left[\alpha_l \mu_{\mathrm{eff},l}\frac{\partial U_{lm}}{\partial x_m}\right] + \alpha_l \rho_l g_i + M_{li} \tag{2}$$

where P is the pressure shared by both gas and liquid phases, $\mu_{\mathrm{eff},l}$ is the effective viscosity of the liquid phase (its calculation procedure is discussed separately in the following subsection) and M_l accounts for the interphase momentum transferred from all the gas bubbles to the liquid phase per unit time per unit volume. The detailed calculation procedure for M_l is discussed in Section 3.2.

The velocity of bubbles can be computed by solving the force balance over the individual bubbles:

$$m_B \frac{\mathrm{d}u_{Bi}}{\mathrm{d}t} = F_{Gi} + F_{Di} + F_{Li} + F_{VMi} + F_{Pi} \tag{3}$$

where m_B is the bubble mass, u_B is the bubble velocity and F_G, F_D, F_L, F_{VM}, F_P are the force due to the gravity, drag force, lift force, virtual mass force and pressure force, respectively. The bubble trajectories can be computed from the bubble velocities as

$$\frac{\mathrm{d}x_{Bi}}{\mathrm{d}t} = u_{Bi} \tag{4}$$

The sum of forces due to the pressure gradient in the liquid phase (F_{Pi}), gravity and buoyancy (F_{Gi}) was calculated as

$$F_{Gi} = m_B g_i \left(1 - \frac{\rho_L}{\rho_B}\right) + \frac{m_B}{\rho_B}\nabla P \tag{5}$$

F_{Di} accounts for the drag force exerted by the liquid on the bubble and was calculated as

$$F_{Di} = \frac{3}{4}\frac{m_B}{\rho_B}\frac{C_D}{d_B}\rho_L(u_{li} - u_{Bi})|u_{li} - u_{Bi}| \tag{6}$$

where u_{li} is the instantaneous liquid velocity and was estimated using Eq. (12). d_B is the bubble diameter. C_D is the drag coefficient and was estimated as (Tsuchiya et al., 1997):

$$C_D = \max\left\{\frac{24}{Re}(1.0 + 0.15Re^{0.687}), \frac{8}{3}\frac{Eo}{Eo+4}\right\} \tag{7}$$

where Re is bubble Reynolds number ($=d_B|U_l - u_B|\rho_l/\mu_l$) and Eo is Eotvos number ($= g\Delta\rho d_B^2/\sigma$). The lift force, F_{Li}, acting on a bubble was calculated as

$$F_{Li} = -C_L \frac{m_B}{\rho_B}\rho_L|u_{li} - u_{Bi}| \times (\nabla \times u_{li}). \tag{8}$$

The virtual mass force, F_{VMi}, acting on a bubble was calculated as

$$F_{VMi} = -\left[\frac{\mathrm{D}I}{\mathrm{D}t} + I \cdot \nabla u_{li}\right] \quad \text{where } I = C_{VM}\rho_l\left(\frac{m_B}{\rho_B}\right)(u_{li} - u_{Bi}) \tag{9}$$

Following Tomiyama et al. (2002), the lift coefficient (C_L) was calculated as

$$C_L = \begin{cases} \min[0.288\tanh(0.121Re), f(Eo_d)] & \text{for } Eo_d < 4 \\ f(Eo_d) & \text{for } 4 \leqslant Eo_d \leqslant 10.7 \end{cases} \tag{10}$$

where

$$f(Eo_d) = 0.0105Eo_d^3 - 0.0159Eo_d^2 - 0.0204Eo_d + 0.474 \tag{11}$$

Following Auton (1983), a virtual mass coefficient (C_{VM}) of 0.5 was used unless mentioned otherwise. There may be other forces acting on bubbles than those mentioned in Eq. (3), such as the Basset force (due to the development of a boundary layer around the bubble), thermophoretic force (due to a large temperature gradient) and Brownian force. The Basset force formulation involves a history integral which makes its estimation computationally intensive. In addition, it is expected to be much smaller than the other dominant forces acting on bubbles and hence it was not included (Ranade, 2002). The magnitudes of other forces such as thermophoretic force and Brownian force are also expected to be very small compared with the magnitude of the forces considered in Eq. (3) and these forces were therefore not considered in the present work.

The instantaneous liquid velocity (u_{li}) used in Eqs. (6), (8) and (9) was estimated as the sum of the mean liquid velocity (U_{li}) and a fluctuating velocity component (u_i') as

$$u_{li} = U_{li} + u_i'(t) \tag{12}$$

In the past, two different models have been used to predict the turbulent dispersion of particles, namely the discrete random walk (DRW) model (Gosman and Ioannides, 1981) and the continuous random walk (CRW) model (Thomson, 1987) which differ in the way in which the instantaneous fluid velocity is estimated from the knowledge of liquid phase turbulence. In the DRW model, the random value of the fluctuating velocity component is kept constant over an interval of time given by the characteristic lifetime of turbulent eddies. In the CRW model, the fluctuating velocity components are obtained by solution of the Langevin equation. This provides a more realistic description of the turbulent eddies, at the expense of increased computational effort (due to the requirement for smaller time steps for the integration of particle trajectory equation). In particular, the CRW model includes the effect of non-isotropic turbulent dispersion and therefore requires more computational resources. Rammohanan et al. (2003) performed single particle trajectory calculations in stirred tanks and their results were not found to be sensitive to the model used for the turbulent dispersion of particles. Therefore, we used the DRW model for the estimation of fluctuating liquid velocity.

In the DRW model, which is also called as the "eddy lifetime model", the fluctuating velocity is added to the mean liquid velocity for a constant time interval given by the characteristic lifetime of liquid eddies. In this case, each eddy was characterized by

(a) the Gaussian distributed random velocity fluctuation u', v' and w', and
(b) the eddy lifetime, τ_e.

The values of u', v' and w' which prevail during the lifetime of the turbulent eddy were assumed to obey a Gaussian distribution during the lifetime of an eddy and were estimated as

$$u' = \zeta\sqrt{u'^2} \tag{13}$$

where ζ is a normally distributed random number and the second term on the RHS of Eq. (13) is the root mean square of local velocity fluctuations, which can be estimated from the local turbulent kinetic energy (k) as (for isotropic turbulence)

$$\sqrt{u'^2} = \sqrt{v'^2} = \sqrt{w'^2} = \sqrt{2k/3} \tag{14}$$

The local turbulent kinetic energy (k) and its dissipation rate (ε) were obtained using the standard k–ε model, which is described in detail later in this section. The characteristic eddy lifetime may be defined as a constant

$$\tau_e = 2T_L \tag{15}$$

or as a random variation about T_L

$$\tau_e = -T_L \log(r) \tag{16}$$

where r is random number from 0 to 1.0. T_L is the integral time scale of turbulence and was estimated from knowledge of the turbulent kinetic energy (k) and turbulent kinetic energy dissipation rate (ε) as (Michaelides, 1997):

$$T_L = 0.15k/\varepsilon \tag{17}$$

The option of random τ_e is known to be more realistic and was therefore used in the present work. The bubble was assumed to interact with the fluid phase eddy over this eddy lifetime. When the eddy lifetime was reached, a new value of the instantaneous velocity was obtained by applying a new value of ζ in Eq. (13).

3.1.1. Turbulence modeling

Several alternatives have been proposed to estimate the effective viscosity of the turbulent liquid phase in gas–liquid flows. The standard k–ε model of turbulence appears to perform satisfactorily (see, for example, Pfleger et al., 1999; Sokolichin and Eigenberger, 1999). In the present work, we therefore used the standard k–ε model to estimate the effective viscosity of liquid phase as

$$\mu_{\mathrm{eff,l}} = \mu_{\mathrm{lam,l}} + \frac{C_\mu \rho_l k^2}{\varepsilon} \tag{18}$$

where $\mu_{\mathrm{eff,l}}$ and $\mu_{\mathrm{lam,l}}$ are the effective and molecular viscosities of the liquid phase, respectively. The modeled form of the liquid phase k and ε transport equation can be written as

$$\frac{\partial}{\partial t}(\alpha_l \phi) + \frac{\partial}{\partial x_i}(\alpha_l U_{li} \phi) = \frac{\partial}{\partial x_i}\left(\alpha_l \frac{\upsilon_t}{\sigma_\phi} \frac{\partial \phi}{\partial x_i}\right) + S_\phi \tag{19}$$

where ϕ can be either k or ε and σ_ϕ is the model parameter describing turbulent dispersion of ϕ. The corresponding source term (S_ϕ) for k and ε can be written as

$$S_k = \alpha_l[(G + G_e) - \varepsilon] \tag{20}$$

$$S_\varepsilon = \alpha_l \frac{\varepsilon}{k}[C_1(G + G_e) - C_2\varepsilon] \tag{21}$$

where C_1 and C_2 are parameters of the k–ε model. Following general practice, we used the same values of these parameters proposed for the single-phase flows ($C_1 = 1.44$, $C_2 = 1.92$, $C_\mu = 0.09$, $\sigma_k = 1.0$, $\sigma_\varepsilon = 1.3$), G is turbulence generation based on velocity gradients in the continuous phase and G_e is an extra turbulence generation due to the presence of the dispersed phase. Lain et al. (2002) analyzed the effect of bubble-induced turbulence on mean and fluctuating liquid and bubble velocities by introducing appropriate source terms in the k and ε equations (Eqs. (20) and (21)). Their results indicate that the incorporation of such source terms in k- and ε-equations leads to better agreement of the predicted and measured quantities. Several investigators have reported that two-dimensional simulations over-predict the turbulent viscosity and therefore damp the low-frequency oscillations (see, for example, Pfleger et al., 1999). Hence, the importance of additional turbulence generation terms used by Lain et al. (2002) in the presence of over-predicted turbulent viscosity due to the two-dimensional nature of simulations is not clearly understood. Kataoka et al. (1992) analyzed the influence of gas bubbles on liquid-phase turbulence. The motion of large bubbles generates extra turbulence. However, their analysis indicates that the extra dissipation due to the small-scale interfacial structures almost compensates for the extra generation of turbulence due to large bubbles. Numerical experiments also indicate that one may neglect the contribution of extra turbulence generation (Ranade, 1997; Pfleger et al., 1999; Sokolichin and Eigenberger, 1999). In the present work, therefore, G_e was set to zero.

3.2. Numerical solution

The numerical simulations were carried out using a rectangular bubble column. This column configuration is same as that used for experiments and Eulerian–Eulerian simulations (Buwa and Ranade, 2003). The simulations were carried out for H/W ratios of 2.25 and 4.5 and superficial gas velocities in the range 0.14–0.73 cm/s. Non-uniform structured grids of 15 (width) × 25 (height) × 5 (depth) cells and $15 \times 46 \times 5$ cells was used for column geometry with H/W ratios of 2.25 and 4.5, respectively, and referred to as coarse grid simulations. Fine grid simulations were carried out using $29 \times 50 \times 11$ and $29 \times 92 \times 11$ computational cells for H/W ratios of 2.25 and 4.5, respectively. Buwa and Ranade (2002) carried out simulations using different configurations of locally aerated spargers and found that the results are not sensitive to the different sparger representations. Therefore, the sparger through which gas was introduced into the column was modeled as the

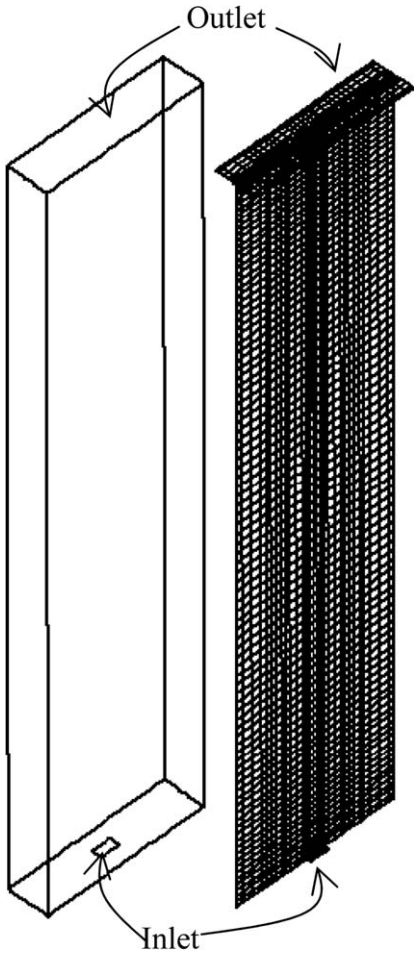

Fig. 2. Typical grid used in present work (H/W: 4.5).

area covered by the sparging holes (18×6 mm in the present case). A typical grid distribution and sparger representation are shown in Fig. 2.

As shown in Fig. 2, the area covering the sparger holes through which gas enters the solution domain is modeled as a velocity inlet. The measured average bubble size was about 5 mm for the range of operating parameters considered in the present work (Buwa and Ranade, 2002). In the simulations, therefore, the rise velocity of bubbles at the inlet was set equal to their terminal rise velocity (0.20 m/s). No-slip boundary conditions were used at all the impermeable walls for the continuous phase, while bubbles were allowed to reflect at these impermeable walls. Formulating boundary conditions at the gas–liquid interface at the top is not straightforward. Ranade (2002) discussed different approaches for formulating the top boundary condition. Following Ranade (2002), in the present work, the top surface of the dispersion was modeled as a velocity inlet. The outgoing (axial) velocity of gas bubbles was set equal to the terminal rise velocity of gas bubbles (estimated from a force balance over a single rising bubble). The normal liquid velocity was set to zero. The implicit assumption here is that gas bubbles escape from the dispersion with their terminal rise velocity. It should be noted that even after defining the top surface as an inlet, the gas volume fraction at the top surface is a free variable. The exact value of the dispersion height was not known a priori. For rectangular bubble columns, since the values of the overall gas volume fraction for the gas velocity values considered in the present work were small ($<2.5\%$ for maximum the gas velocity of 0.73 cm/s used in this work), the height of the dispersion was set equal to the height of the clear liquid in all the simulations.

The model equations presented above were solved using the commercial flow simulation software FLUENT 6.1 (Fluent Inc., USA). The user-defined drag and lift force (defined by Eqs. (6)–(8)) were supplied through appropriate user-defined functions (UDFs). Separate time-averaging procedures were also incorporated using user-defined functions. The spatial derivative terms were discretized using a second-order QUICK discretization scheme (see Leonard, 1979, and FLUENT user manuals) whereas temporal derivatives were discretized using a first-order scheme. An Eulerian time step of 0.01 s was used in all simulations. All the simulations were performed on a dual processor machine with Intel PIV processors. A typical transient 3-D simulation carried with a fine grid ($29 \times 92 \times 11$ cells) took about 5–6 days of computing. It should be noted that the transient simulations need to be carried out for several plume oscillation cycles in order to obtain a reasonably well-developed time-averaged flow after discarding initial transients. Owing to hardware limitations, simulations could not be performed with further grid refinement.

The time step used to integrate the equations of bubble motion was calculated as

$$\Delta t_{\mathrm{L}} = \frac{\Delta t^*}{\lambda} \tag{22}$$

where Δt^*, is the characteristic time that is related to an estimate of the time required for the bubble to traverse the current continuous phase control volume and λ is the user-supplied step length factor, which is roughly equal to the number of time steps required to traverse the continuous phase control volume. The effect of step length factor on key dynamic and time-averaged flow properties is discussed in Section 4. A step length factor of 100 was used unless mentioned otherwise. The number of bubbles tracked was typically in the range 300–5500 for the range of superficial gas velocities and H/W ratios considered. The bubble positions were updated after each iteration of the continuous phase. About 100 internal iterations were carried out for each continuous phase iteration to ensure convergence.

The coupling between the dispersed and continuous phases is achieved through the liquid volume fraction ($\alpha_{\mathrm{l}} = 1 - \alpha_{\mathrm{g}}$) and momentum transfer from bubbles to liquid ($M_{\mathrm{l}i}$). Both the gas volume fraction (α_{g}) and momentum source term needs to be summed over the number of bubbles present in the computational cell. The local liquid velocity at the centre of the bubble mass position used in Eqs. (6)–(8) needs to be calculated from the Eulerian nodes of the computational cell. The gas phase volume fraction was calculated as the ratio of the sum of the volume of bubbles (V_{B}) in the computational cell under consideration to the cell volume (V_{cell}):

$$\alpha_{\mathrm{g}} = \frac{\sum_n V_{\mathrm{B}i}}{V_{\mathrm{cell}}} \tag{23}$$

where n is the number of bubbles. The momentum transferred from each bubble was calculated as the sum of instantaneous momentum contributions along the bubble trajectory in the control volume at each Lagrangian time step as

$$M_{\mathrm{l}i} = -\frac{1}{V_{\mathrm{cell}}\,\Delta t_{\mathrm{E}}} \sum_n \sum_k (F_{\mathrm{D}i} + F_{\mathrm{L}i} + F_{\mathrm{VM}i})\Delta t_{\mathrm{L}} \tag{24}$$

where V_{cell} is the control volume size. Δt_{E} and Δt_{L} are Eulerian and Lagrangian time steps, respectively, and $F_{\mathrm{D}i}$, $F_{\mathrm{L}i}$ and $F_{\mathrm{VM}i}$ represent the momentum transfer through drag, lift and virtual mass force, respectively. The summation over k represents the sum of the instantaneous momentum contributions along the bubble trajectory in the control volume and summation over n accounts for the number of bubbles passing through the control volume under consideration.

4. Results and discussion

When gas is introduced into the column filled with liquid, gas bubbles formed at the sparger holes rise upwards in the pool of liquid exhibiting different length and time scales. Experimental instantaneous snapshots of the oscillating bubble plume are shown in Fig. 3(a)(i) and (b)(i) for superficial gas velocities of 0.14 and 0.73 cm/s, respectively. The inherently unsteady flow around individual bubbles eventually leads to gross recirculatory flow as shown in Fig. 3. The focus of present work was to develop computational models

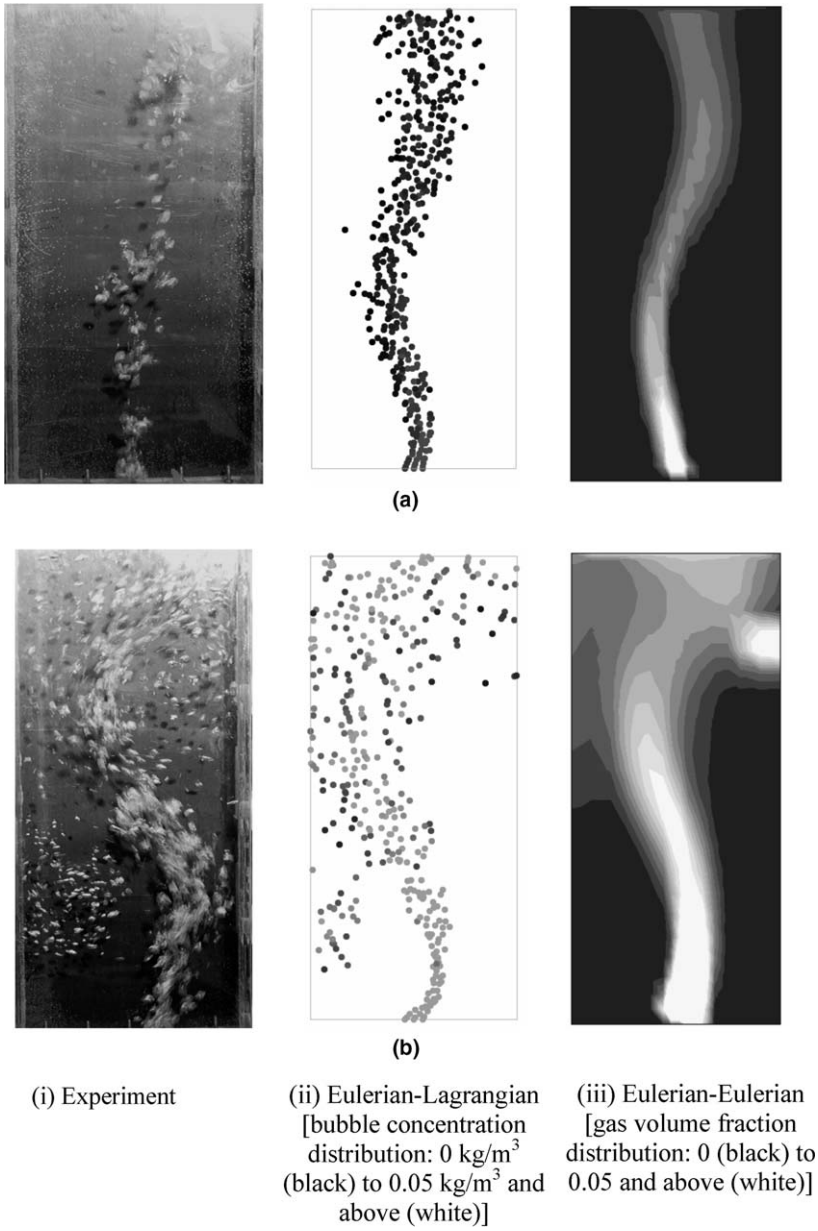

Fig. 3. Experimental and simulated snapshots of meandering bubble plume at a superficial gas velocity of (a) 0.14 and (b) 0.73 cm/s (H/W: 2.25).

based on the Eulerian–Lagrangian approach to characterize the low-frequency oscillations of the meandering bubble plume and bubble scale information.

The numerical simulations were carried out for a column with an H/W ratio of 2.25 for superficial gas velocities in the range 0.14–0.73 cm/s. Initial simulations were carried out using a coarse grid ($15 \times 5 \times 25$ cells). In these simulations, momentum exchange was accounted for through drag and virtual mass forces (Eq. (3)). The typical instantaneous distributions of bubbles obtained using Eulerian–Lagrangian simulation at superficial gas velocities of 0.14 and 0.73 cm/s (at an H/W ratio of 2.25) are shown in Fig. 3(a)(ii) and (b)(ii). In our previous work (Buwa and Ranade, 2003), we have also carried out Eulerian–Eulerian simulations for the same column geometry, operating conditions and model parameters and the predicted instantaneous gas

volume fraction distribution is shown in Fig. 3(a)(iii) and (b)(iii). It can be seen from the figures that the meandering motion of the bubble plume is captured in satisfactory qualitative agreement with the experiments and the instantaneous gas volume fraction distribution obtained using the Eulerian–Eulerian simulations. In order to make a quantitative comparison of simulated results with experimental measurements, the plume oscillation

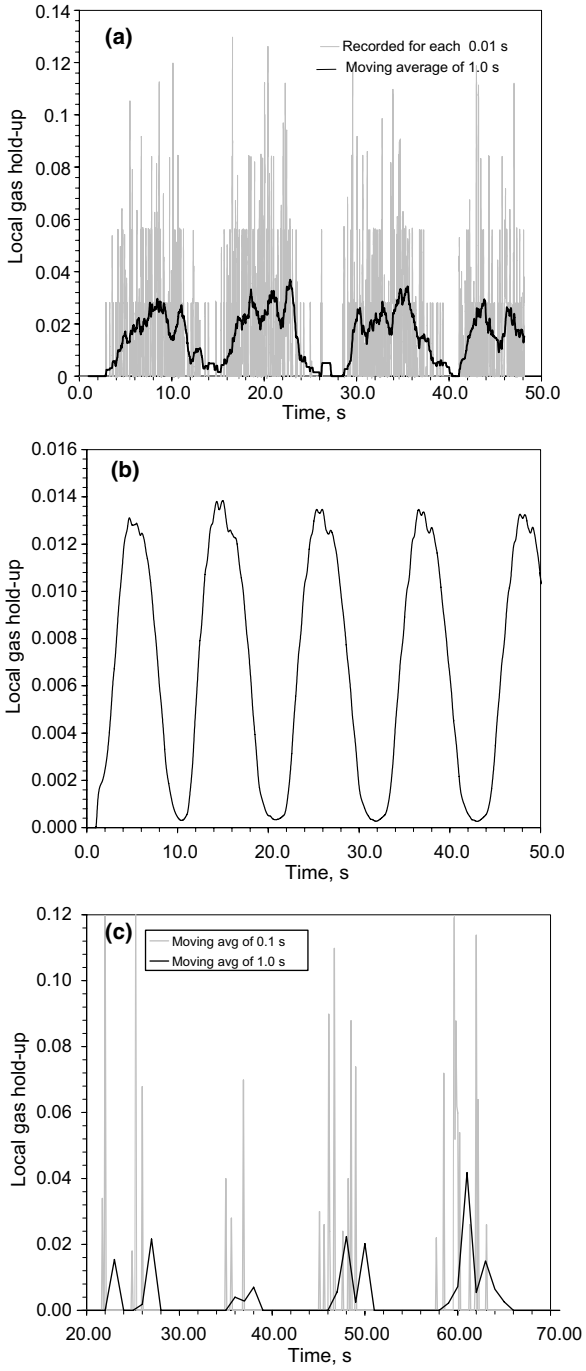

Fig. 4. Voidage fluctuation time series obtained from (a) Eulerian–Lagrangian, (b) Eulerian–Eulerian simulations and (c) experiment (superficial gas velocity: 0.14 cm/s; H/W: 2.25).

period and time-averaged flow properties (vertical liquid velocity and gas hold-up) were compared with the experimental measurements.

4.1. H/W ratio of 2.25

The voidage fluctuation time series simulated using the Eulerian–Lagrangian approach at a superficial gas velocity of 0.14 cm/s, an H/W ratio of 2.25 and recorded at $X = 0.1$ m, $Y = 0.25$ m and $Z = 0.025$ m is shown in Fig. 4(a), the corresponding time series predicted using the Eulerian–Eulerian model is shown in Fig. 4(b) and the experimentally recorded voidage fluctuation time series using the conductivity probe is shown in Fig. 4(c). The low-frequency oscillations corresponding to motion of meandering bubble plume can be clearly seen and the number of low-frequency oscillations predicted by both Eulerian–Lagrangian and Eulerian–Eulerian models were in good agreement with the experimental observations. The number of low frequency oscillations predicted by the Eulerian–Lagrangian approach is about 4 (in 50 s after discarding the initial transients) (Fig. 4(a)), whereas that predicted by the Eulerian–Eulerian approach is about 4.5 (Fig. 4(b)). It should be noted that the plume oscillation behavior is not exactly periodic (all cycles do not have the same plume oscillation period). In fact, a distribution of the plume oscillation period always exists both in experiments and in simulations. To analyze the experimental data, we used the dominant frequency of the power spectrum to calculate the mean plume oscillation period. To analyze CFD simulations, we calculated the plume oscillation period by averaging over a large number of cycles. When the number of cycles considered for averaging is greater than 10, the average value of plume oscillation period remains almost the same.

In the case of voidage fluctuation time series obtained using the Eulerian–Lagrangian approach (as shown in Fig. 4(a)), the gas hold-up fluctuation time series is constructed based on the passage of bubbles at a predefined position in the column. Further, the averaging needs to be done with a suitably defined characteristic time scale to extract the Eulerian information. Such averaged gas hold-up fluctuation time series obtained using two different characteristic time scales are shown in Fig. 4(a). For more adequate comparison, we compared the plume oscillation period, defined as the time required for one plume oscillation, with the experimentally measured plume oscillation period, as shown in Fig. 5. Satisfactory agreement can be seen for a range of superficial gas velocities. This also agrees well with the oscillation periods predicted by the Eulerian–Eulerian approach.

Before investigating the effect of various models and parameters, we studied the adequacy of the Lagrangian time step (Δt_L) estimated using Eq. (22). We carried out simulations using step length factors (λ in Eq. (22)) of 20 and 100 to study its effect on the plume oscillation period. At a superficial gas velocity of 0.14 cm/s, the predicted plume oscillation period was not affected by λ. However, at a superficial gas velocity of 0.73 cm/s,

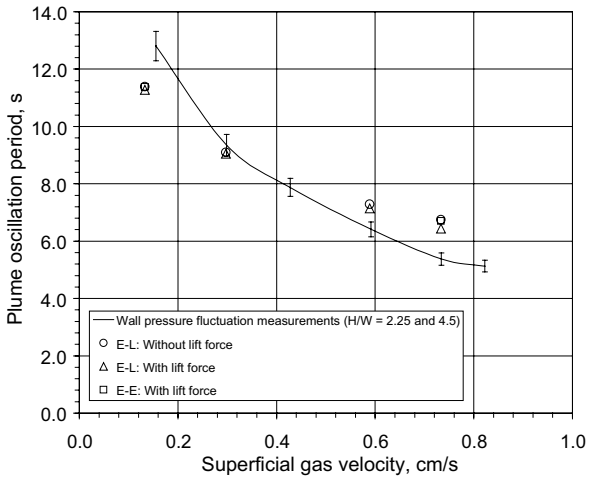

Fig. 5. Effect of superficial velocity on plume oscillation period at an H/W ratio of 2.25 [wall pressure fluctuation measurements of Buwa and Ranade (2002) for H/W ratios of 2.25 and 4.5, Eulerian–Eulerian simulations of Buwa and Ranade (2003)].

the plume oscillation period was obtained using a step length factor of 20 was 7.23 s and that obtained using a step length factor of 100 was 6.73 s (compared with an experimentally observed plume oscillation period of 5.88 s). With an almost fivefold increase in step length factor, only a 7% improvement in the predicted plume oscillation period was observed. Therefore, we used a step length factor of 100 in further simulations. We also studied the effect of grid resolution, lift and virtual mass force on the predicted plume oscillation period and time-averaged flow properties at different superficial gas velocities and H/W ratios and the results are discussed in the following sections.

The comparison of experimentally measured and predicted time-averaged gas hold-up and vertical liquid velocity profiles is shown in Fig. 6(a) and (b) for a superficial gas velocity of 0.14 cm/s (for an H/W ratio of 2.25). Fig. 6(a) shows a comparison of the experimentally measured time-averaged gas hold-up (see Buwa and Ranade, 2005, for details of experiments) and predicted results at a liquid height of 0.37 m from the column bottom. The time-averaged vertical velocity measured by Pfleger et al. (1999) for the same column geometry was used for validation of the predicted time-averaged vertical liquid velocity, as shown in Fig. 6(b). The comparison of the predicted gas hold-up with the experiments of Buwa and Ranade (2005) at a superficial gas velocity of 0.73 cm/s is shown in Fig. 7. Unfortunately, experimental data on the time-averaged liquid velocity were not available for this gas velocity. It should noted that the asymmetry in the measured gas hold-up profiles as seen from Fig. 6(a) is a result of an insufficient data acquisition time.

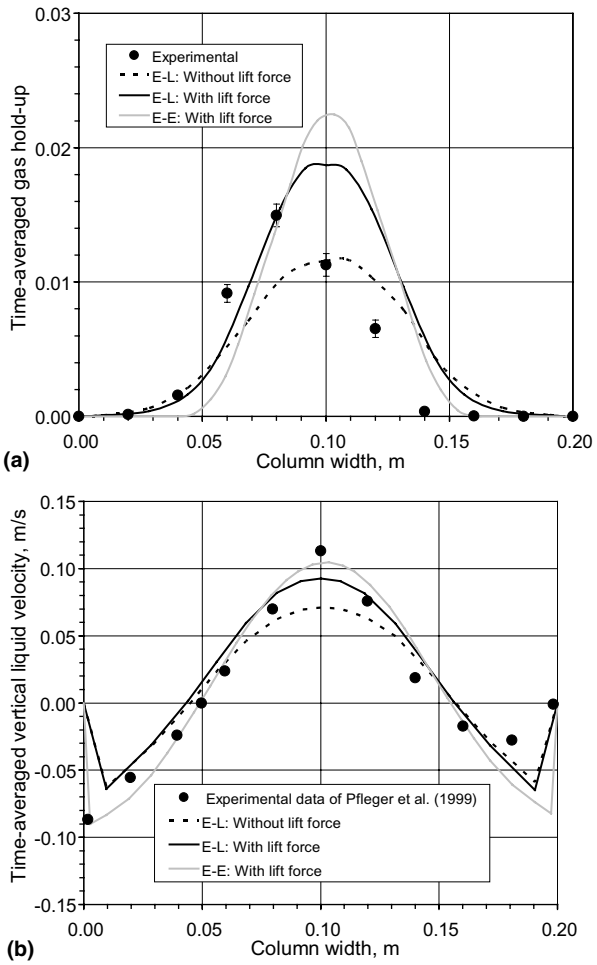

Fig. 6. Time-averaged gas hold-up and vertical liquid velocity profiles predicted using Eulerian–Lagrangian simulations at an H/W ratio of 2.25 and a superficial gas velocity of 0.14 cm/s ($Y = 0.37$ m). (a) Time-averaged gas hold-up and (b) time-averaged vertical liquid velocity (experiments of Buwa and Ranade (2005) and Eulerian–Eulerian simulations of Buwa and Ranade, 2003).

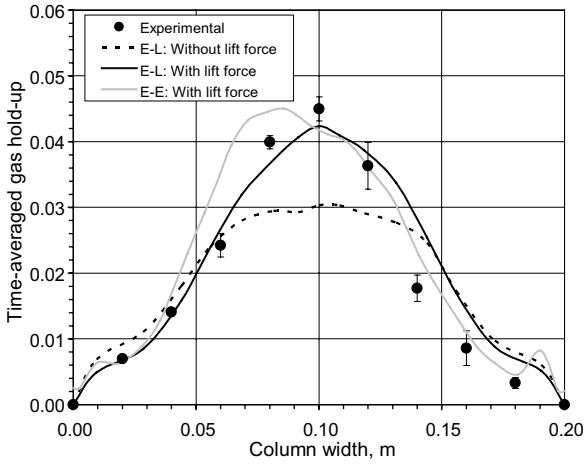

Fig. 7. Time-averaged gas hold-up profiles predicted using Eulerian–Lagrangian simulations at an H/W ratio of 2.25 and superficial gas velocity of 0.73 cm/s ($Y = 0.37$ m) (experiments of Buwa and Ranade, 2005 and Eulerian–Eulerian simulations of Buwa and Ranade, 2003).

Particularly for low superficial gas velocities (as shown in Fig. 6(a)), where the plume spread is narrow, the plume oscillation period is sufficiently large and it is difficult to acquire the experimental data for a very long time to obtain symmetric gas hold-up profiles. However, as observed from Fig. 7, at larger superficial gas velocities, the plume oscillation period is smaller and also the plume disperses reasonably and therefore the gas hold-up profiles are symmetric. It can be seen from Figs. 6 and 7 that simulations carried without virtual mass and lift force under-predict the time-averaged flow properties. Therefore, we carried out further simulations to study the importance of virtual mass and lift force.

We carried out simulations without and with virtual mass force (with a C_{VM} of 0.5). It was observed that neither the plume oscillation period nor the time-averaged properties (vertical liquid velocity and gas hold-up) were sensitive to the virtual mass force. This also agrees with the Eulerian–Eulerian simulations of Buwa and Ranade (2003). We examined the effect of lift force using the lift coefficient correlation proposed by Tomiyama et al. (2002) (see Eqs. (10) and (11)). The lift coefficient estimated from this correlation for a bubble size of 5 mm is about 0.2 (compared with a classical lift coefficient value of 0.5 used in previous studies; for example, see Delnoij et al., 1997a,b). As shown in Fig. 5, the predicted plume oscillation period was not affected by the

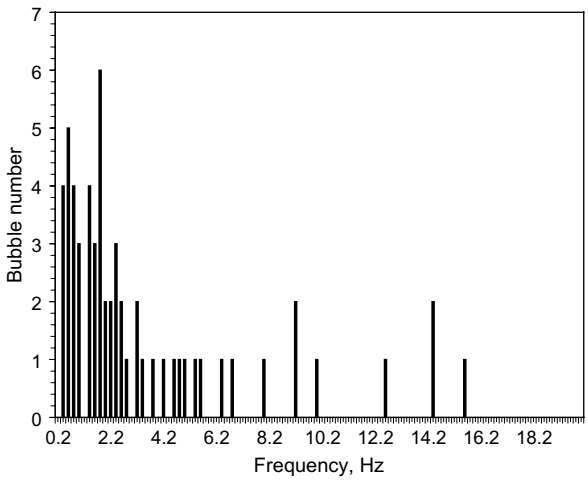

Fig. 8. Distribution of bubble passage frequencies at 0.73 cm/s at $X = 0.1$ m, $Y = 0.25$ m and $Z = 0.025$ m (H/W: 2.25).

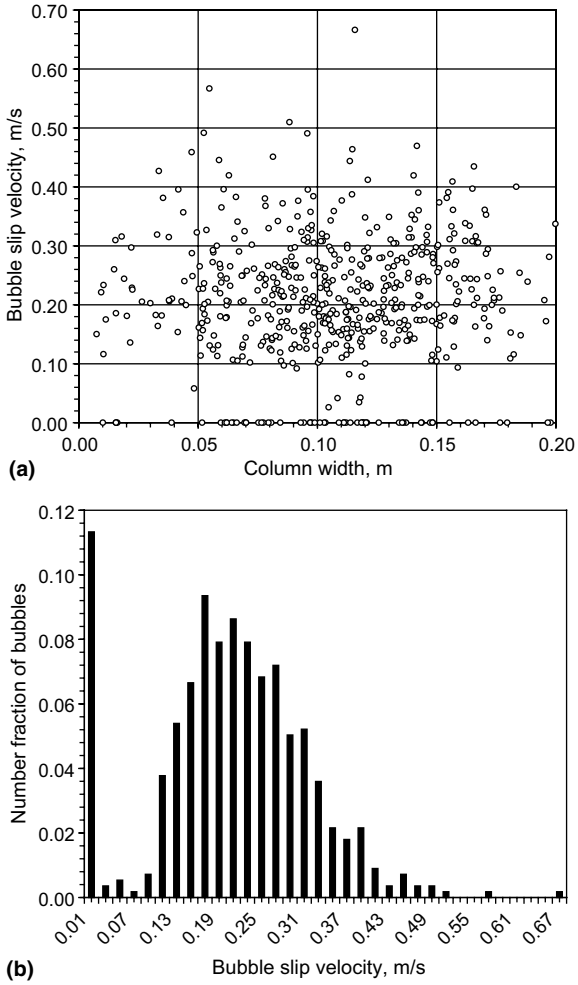

Fig. 9. (a) Bubble slip velocity distribution along column width and (b) histogram of bubble slip velocity (superficial gas velocity: 0.73 cm/s; $Y = 0.37$ m, H/W: 2.25).

lift force for an H/W ratio of 2.25 for superficial gas velocities up to 0.59 cm/s. For superficial gas velocities greater than 0.59 cm/s, the velocity gradients in the liquid phase become significant and the effect of lift force starts to become evident. Further, the plume oscillation periods predicted by both the Eulerian–Lagrangian and Eulerian–Eulerian approaches are almost the same and agree well with the measurements. However, it can be seen from Figs. 6 and 7 that the lift force is necessary for the accurate prediction of time-averaged flow properties. The effect of lift force is more significant for higher H/W ratios and is discussed further in the following section.

In addition to the Eulerian–Eulerian simulations, additional bubble scale information was obtained in the Eulerian–Lagrangian simulations. In order to extract bubble scale information such as bubble passage frequency and bubble slip velocity, we recorded bubbles crossing a particular plane in the column (at a dispersed liquid height of $Y = 0.25$ m) and computed bubble passage frequency (defined as the reciprocal of the time between successive passages of bubbles) at a specific location on the plane ($X = 0.1$ m, $Y = 0.25$ m, and $Z = 0.025$ m) and its distribution is shown in Fig. 8. The predicted time-averaged bubble passage frequency of 2 Hz agrees well with the experimental results of Buwa and Ranade (2005). The instantaneous bubble slip velocity and its distribution recorded for about 550 bubbles at any particular instant at a superficial gas velocity of 0.73 cm/s are shown in Fig. 9(a). Even though the mean slip velocity was 0.2054 m/s,

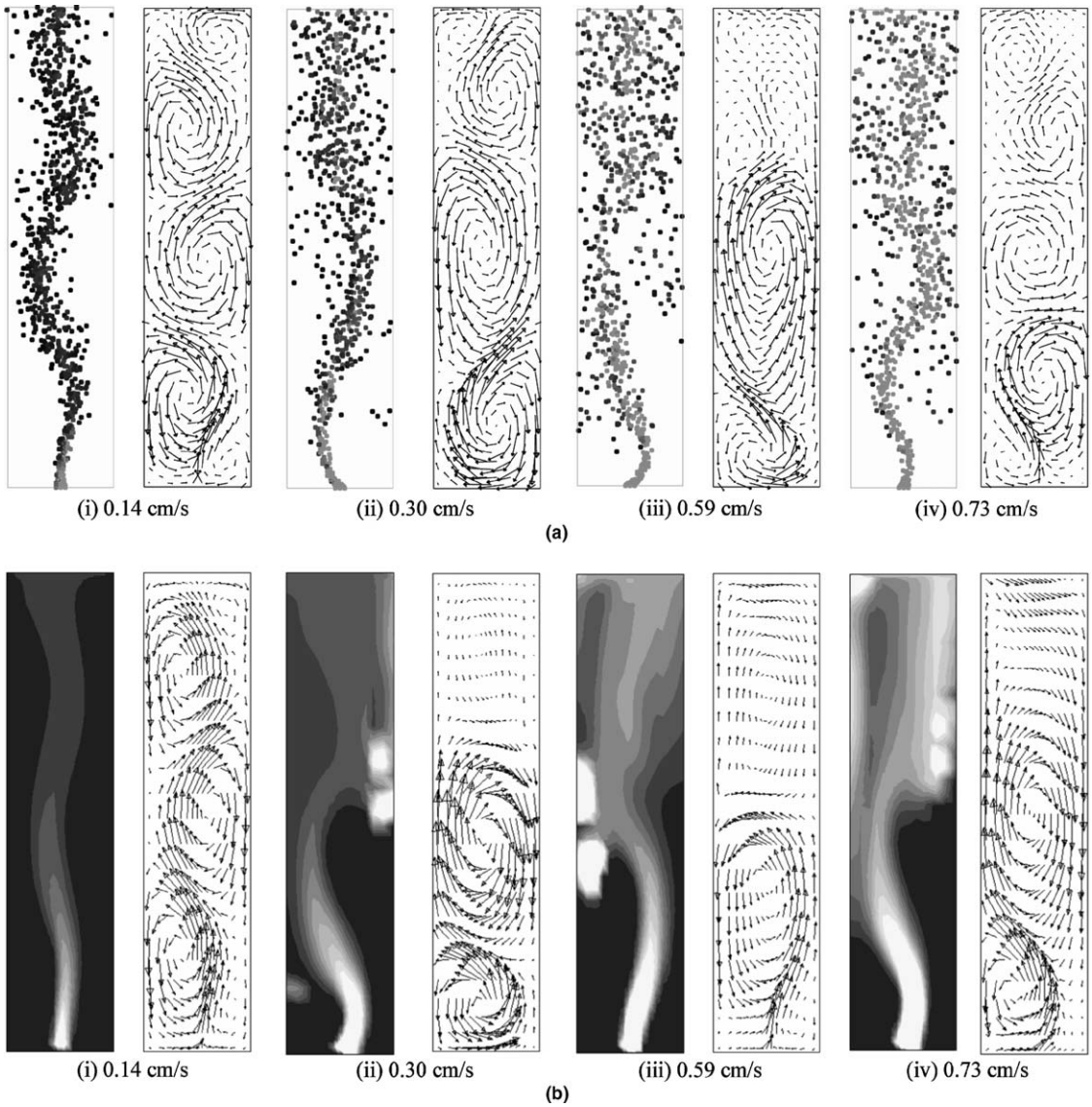

Fig. 10. Effect of numerical diffusion on the dynamics of meandering bubble plume (coarse grid, H/W: 4.5). (a) Eulerian–Lagrangian simulations without lift force [Instantaneous bubble distribution [10 uniform contours of particle concentration in kg/m^3 between 0 (black) and 0.05 and above(white)] and instantaneous liquid velocity field (maximum velocity corresponds to 0.6 m/s)] and (b) Eulerian–Eulerian simulations of Buwa (2004) with a lift coefficient of 0.5 [Instantaneous gas volume fraction distribution [10 uniform contours between 0.0 (black) and 0.05 and above (white)] and instantaneous liquid velocity field (maximum velocity corresponds to 0.6 m/s)].

which agrees well for the bubbles of 5 mm diameter, there is a significant variation of slip velocities about this mean value, as shown in Fig. 9(b).

4.2. H/W ratio of 4.5

The effect of H/W ratio was also studied. Fig. 10(a) shows instantaneous bubble positions and liquid velocity distribution at an H/W ratio of 4.5 simulated using a coarse grid and without lift force at superficial gas velocities of 0.14, 0.30, 0.59 and 0.73 cm/s. It can be seen from Fig. 10(a) that the local recirculation is correctly captured for low gas velocities (up to 0.30 cm/s). For higher gas velocities (0.59 and 0.73 cm/s), however, the local recirculation in the upper part of the column is not clearly predicted. In order to investi-

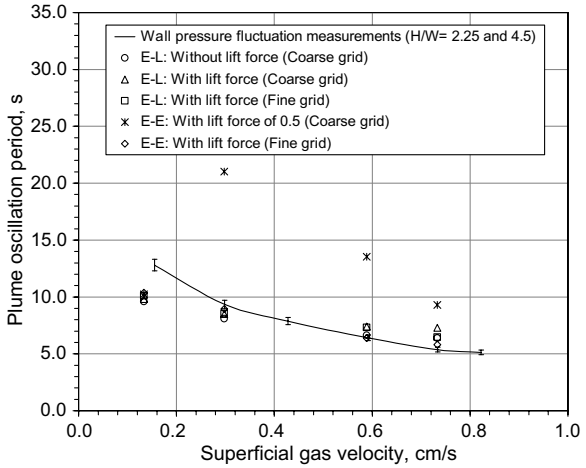

Fig. 11. Effect of superficial velocity on plume oscillation period at an H/W ratio of 4.5 [wall pressure fluctuation measurements of Buwa and Ranade (2002) for H/W ratios of 2.25 and 4.5, Eulerian–Eulerian simulations of Buwa and Ranade (2003)].

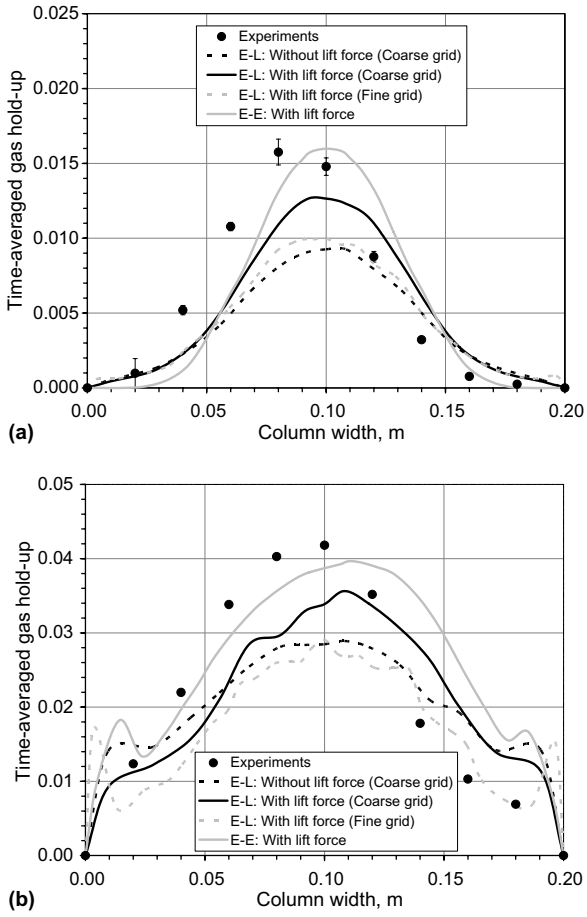

Fig. 12. Time-averaged gas hold-up profiles predicted using Eulerian–Lagrangian simulations at an H/W ratio of 4.5 and a superficial gas velocity of (a) 0.14 and (b) 0.73 cm/s ($Y = 0.675$ m) (experiments of Buwa and Ranade (2005), and Eulerian–Eulerian simulations of Buwa and Ranade (2003)).

gate further, we calculated the plume oscillation period from the numerically predicted voidage fluctuation time series and the results are shown in Fig. 11. It should be noted that the measured plume oscillation periods for H/W ratios of 2.25 and 4.5 were almost same (Buwa and Ranade, 2004) and measurements lie within the error bar shown in Fig. 11. We also compared the predicted long time-averaged gas hold-up profiles with the measurements of Buwa and Ranade (2005) for superficial gas velocities of 0.14 and 0.73 cm/s as shown in Fig. 12(a) and (b), respectively. Unfortunately, the time-averaged liquid velocity data were not available for this H/W ratio. Although the numerically predicted plume oscillation periods agree well with the measured vales (as shown in Fig. 11), it can be seen from Fig. 12(a) and (b) that the gas hold-up is

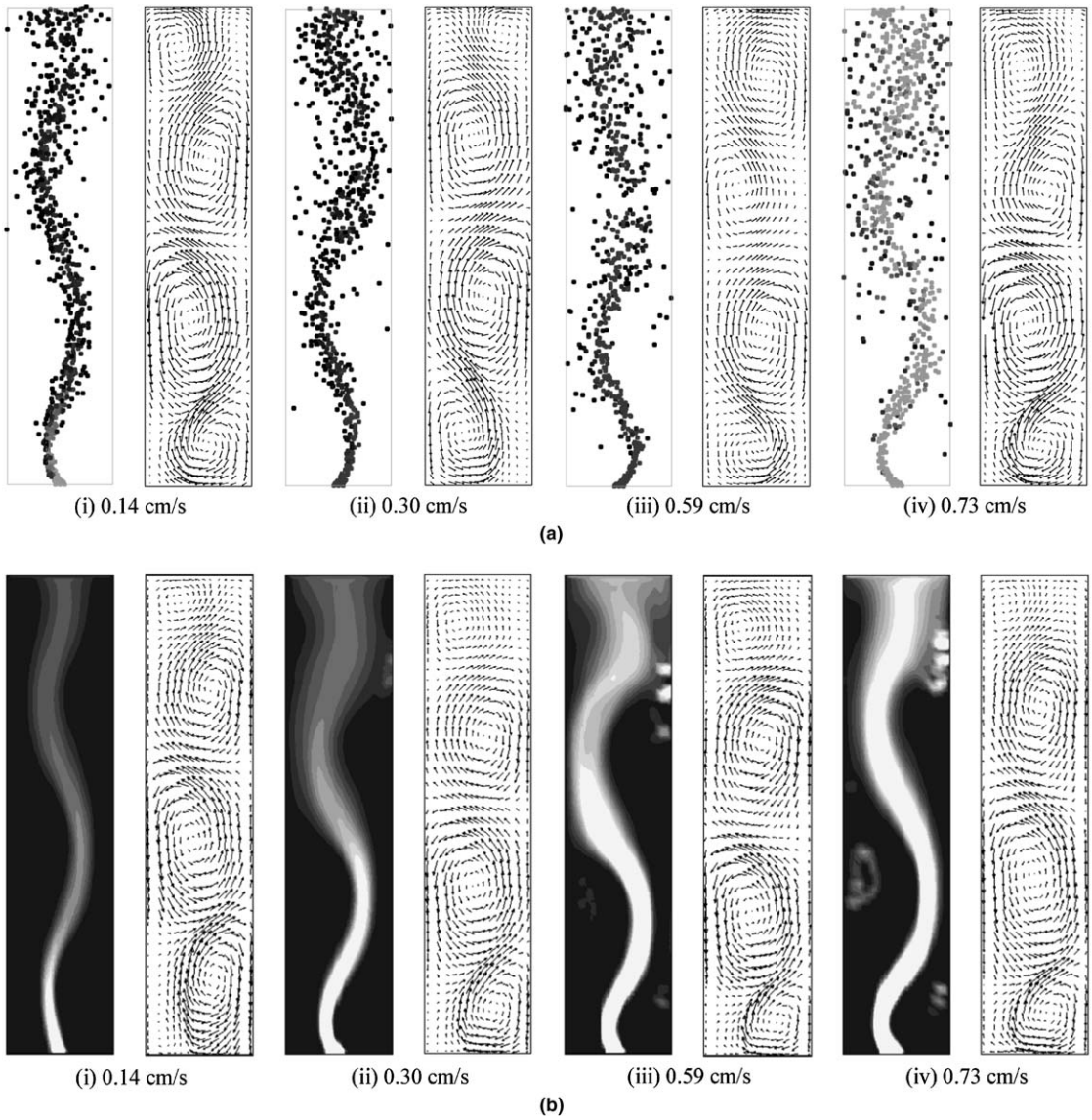

Fig. 13. Effect of lift force on the dynamics of meandering bubble plume [fine grid, with lift coefficient of Tomiyama et al. (2002), H/W: 4.5]. (a) Eulerian–Lagrangian simulations [instantaneous bubble distribution [10 uniform contours of particle concentration in kg/m^3 between 0 (black) and 0.05 and above (white)] and instantaneous liquid velocity field (maximum velocity corresponds to 0.6 m/s)] and (b) Eulerian–Eulerian simulations of Buwa and Ranade (2003) [instantaneous gas volume fraction distribution [10 uniform contours between 0.0 (black) and 0.05 and above (white)] and instantaneous liquid velocity field (maximum velocity corresponds to 0.6 m/s)].

under-predicted for simulations carried without considering the lift force. It is therefore necessary to include the lift force.

In addition to the effect of lift force, the role of numerical diffusion, which is more pronounced in the Eulerian–Eulerian simulations, is also important. For example, it can be seen from the results of Eulerian–Eulerian simulations (as shown in Fig. 10(b)) carried out using the coarse grid and the classical value of the lift coefficient of 0.5 that the numerical diffusion and excess lateral migration of gas bubbles caused by higher value of lift coefficient lead to gas accumulation near the column walls and breakdown of the local recirculatory flow. The combined effect of numerical diffusion and the incorrect magnitude of the lift force on the dynamics can be further demonstrated from the plume oscillation periods obtained using the coarse grid Eulerian–Eulerian simulation as shown in Fig. 11. It can be seen that the plume oscillation periods are severely over-predicted at higher gas velocities. In addition to the plume oscillation period, the numerical diffusion and incorrect lift force lead to gas accumulation near the column walls in the upper part of the column. These effects of gas accumulation near the column walls were further discussed by Buwa and Ranade (2003). Hence it should noted that a reduction in numerical diffusion (by the use of a finer grid) and correct modeling of the lift force are key factors in predicting the dynamic and time-averaged flow characteristics of unsteady gas–liquid flows. Since the motion of individual bubbles is simulated in the Lagrangian approach, the numerical diffusion is much lower than in the Eulerian–Eulerian approach which is based on the solution of averaged equations.

Based on our previous work on Eulerian–Eulerian simulations (Buwa and Ranade, 2003), we further investigated the role of lift force by using the correlation of Tomiyama et al. (2002) for the calculation of lift force. For a further quantitative comparison, we compared the predictions of the coarse grid Eulerian–Lagrangian simulations carried out accounting for the lift force with the measured plume oscillation period and time-averaged gas hold-up profiles. The simulations carried out accounting for the lift force led to improved agreement between the predicted and measured gas hold-up profiles (see Fig. 12(a) and (b)), but adversely affected the predictions of the plume oscillation period at superficial gas velocities of 0.59 and 0.73 cm/s, as shown in Fig. 11. In order to assess the role of numerical diffusion, we further carried out the simulations using a fine grid resolution ($29 \times 92 \times 11$ cells). The simulated instantaneous bubble positions and liquid velocity distribution are shown in Fig. 13(a). It can be seen the liquid recirculation in the top of the column at higher liquid velocities is now captured well. The corresponding Eulerian–Eulerian predictions of Buwa and Ranade (2003) are also shown in Fig. 13(b). It can be seen that the Eulerian–Lagrangian simulations correspond well with these simulations. It is interesting that although the plume oscillation periods are better predicted with grid refinement, the agreement between predicted and measured gas hold-up profiles deteriorated (see Figs. 11 and 12).

Pfleger and Becker (2001) and Buwa and Ranade (2002) discussed the effects of grid resolution on both dynamic and time-averaged flow properties (gas hold-up and liquid velocity profiles) and also reported that the agreement of the predicted results with the experiments deteriorates with grid refinement. Unfortunately, since liquid velocity measurements are not available for higher H/W ratios, it is difficult to assess the overall quality of predictions. Its should be noted that the numerical diffusion in coarse grid simulations suppresses the effect of many of the physical models [for example, the inter-phase coupling forces (such as lift and virtual mass force), the turbulence dispersion of gas bubbles or the modulation of turbulence due to the presence of bubbles]. However, with grid refinement, the numerical diffusion is significantly reduced, although not eliminated, and the effects of physical models mentioned above become evident. The effect of the magnitude of different inter-phase coupling forces and other physical models should, in principle, be verified at a refined grid. However, simulations with grid refinement are possible only for a few cycles of plume oscillation. Further, reasonable time-averaged profiles can be obtained only after time-averaging over several cycles. Further work is in progress to investigate the role of numerical diffusion using refined grid resolutions and to account for the effect of the dispersed phase gas volume fraction, which will be reported separately.

5. Conclusions

The dynamics of gas–liquid flows in rectangular bubble columns was studied using Eulerian–Lagrangian simulations. The low-frequency oscillations corresponding to oscillatory motion of the bubble plume were

accurately captured and the plume oscillation period was in good agreement with the experimental measurements and with the Eulerian–Eulerian predictions of Buwa and Ranade (2003). The comparison of the predicted time-averaged gas hold-up and vertical liquid velocity with experimental measurements and Eulerian–Eulerian simulations was found to be satisfactory. For higher H/W ratios, it was observed that the numerical diffusion and incorrect magnitude of lift force lead to breakdown of local recirculatory flow in the upper part of the column. Although we attempted to compare the predicted bubble-scale information, for example, bubble passage frequency, additional measurements on bubble rise velocity are necessary for rigorous validation of Eulerian–Lagrangian models. Further work is also necessary to examine the effects of grid resolution and the effect bubble-induced turbulence in more detail. The present work would provide a basis for such further work.

Acknowledgements

One of the authors (V.V.B.) is grateful to the CSIR, New Delhi, for providing a research fellowship and to the Institute of Fluid Mechanics (LSTM), University of Erlangen—Nuremberg, Germany for the support received during completion of this manuscript. The authors are grateful to Dr. R.V. Chaudhari of NCL, Pune, and Professor V.A. Juvekar of IIT, Bombay, for helpful discussions, and gratefully acknowledge the help of Mr. Mohan R. Rampure in the preparation of this manuscript. The Department of Science and Technology (Grant DST/SF/40/99) supported part of this work.

References

Auton, T.R., 1983. The dynamics of bubbles, drops and particles in motion in liquids. Ph.D. thesis. University of Cambridge, Cambridge, UK.

Becker, S., Sokolichin, A., Eigenberger, G., 1994. Gas–liquid flow in bubble columns and loop reactors: Part II. Comparison of detailed experiments and flow simulations. Chem. Eng. Sci. 49, 5747.

Buwa, V.V., 2004. Modeling of gas–liquid flows in bubble columns. Ph.D. thesis. Indian Institute of Technology—Bombay, Mumbai, India.

Buwa, V.V., Ranade, V.V., 2002. Dynamics of gas–liquid flows in rectangular bubble columns: experiments and single/multi-group simulations. Chem. Eng. Sci. 57, 4715.

Buwa, V.V., Ranade, V.V., 2003. Mixing in bubble columns reactors: role of unsteady flow structures. Canad. J. Chem. Eng. 81, 402.

Buwa, V.V., Ranade, V.V., 2004. Characterization of dynamics of gas–liquid flows in rectangular bubble columns. Am. Inst. Chem. Engr. J. 50, 2394.

Buwa, V.V., Ranade, V.V., 2005. Characterization of gas–liquid flows in rectangular bubble columns using conductivity probes. Chem. Eng. Commun. 192, 1129.

Delnoij, E., Lammers, F.A., Kuipers, J.A.M., van Swaaij, W.P.M., 1997a. Dynamic simulation of dispersed gas–liquid two-phase flow using a discrete bubble model. Chem. Eng. Sci. 52, 1429.

Delnoij, E., Kuipers, J.A.M., van Swaaij, W.P.M., 1997b. Dynamic simulation of gas–liquid two-phase flow: effect of column aspect ratio on the flow structure. Chem. Eng. Sci. 52, 3759.

Delnoij, E., Kuipers, J.A.M., van Swaaij, W.P.M., 1999. A three-dimensional CFD model for gas–liquid bubble columns. Chem. Eng. Sci. 54, 2217.

Gosman, A.D., Ioannides, E., 1981. Aspects of computer simulation of liquid fueled combustors. In: Proceedings of 19th Aerospace meeting, AIAA, St. Louis, MO, Paper No. 81-03223.

Kataoka, I., Besnard, D.C., Serizawa, A., 1992. Basic equation of turbulence and modeling of interfacial terms in gas–liquid two phase flows. Chem. Eng. Commun. 118, 221.

Lain, S., Broder, D., Sommerfeld, M., 1999. Experimental and numerical studies of the hydrodynamics in a bubble column. Chem. Eng. Sci. 54, 4913.

Lain, S., Broder, D., Sommerfeld, M., Goz, M.F., 2002. Modelling hydrodynamics and turbulence in a bubble column using the Euler–Lagrange procedure. Int. J. Multiphase Flow 28, 1381.

Lapin, A., Lubbert, A., 1994. Numerical simulation of the dynamics of two phase gas–liquid flows in bubble columns. Chem. Eng. Sci. 49, 3661.

Leonard, B.P., 1979. A stable and accurate convective modeling procedure based on quadratic upstream interpolation. Comput. Meth. Appl. Mech. Eng. 19, 59.

Michaelides, E.E., 1997. Review—The transient equation of motion for particles, bubbles, and droplets. J. Fluids Eng. 119, 233.

Pfleger, D., Becker, S., 2001. Modelling and simulation of the dynamic flow behavior in a bubble column. Chem. Eng. Sci. 56, 1737.

Pfleger, D., Gomes, S., Gilbert, N., Wagner, H.-G., 1999. Hydrodynamic simulations of laboratory scale bubble columns. Fundamental studies of the Eulerian–Eulerian modeling approach. Chem. Eng. Sci. 54, 5091.

Rammohanan, A.R., Dudukovic, M.P., Ranade, V.V., 2003. Eulerian flow field estimation from particle trajectories: numerical experiments for stirred tank type flows. Indust. Eng. Chem. Res. 42, 2589.

Rampure, M.R., Buwa, V.V., Ranade, V.V., 2003. Modelling of gas–liquid/gas–liquid–solid flows in bubble column reactors. Canad. J. Chem. Eng. 81, 692.

Ranade, V.V., 1997. Modelling of turbulent flow in a bubble reactor. Chem. Eng. Res. Des. 75, 14.

Ranade, V.V., 2002. Computational Flow Modelling for Chemical Reactor Engineering. Academic Press, London.

Sokolichin, A., Eigenberger, G., 1999. Applicability of standard k–ε turbulence model to the dynamic simulation of bubble columns. Part I. Detailed numerical simulations. Chem. Eng. Sci. 54, 2273.

Sokolichin, A., Eigenberger, G., Lapin, A., Lubbert, A., 1997. Dynamic numerical simulation of gas–liquid two-phase flows: Euler–Euler versus Euler–Lagrange. Chem. Eng. Sci. 52, 611.

Thomson, D.J., 1987. Criteria for the selection of stochastic models of particle trajectories in turbulent flows. J. Fluid Mech. 180, 529.

Tomiyama, A., Tamaia, H., Zun, I., Hosokawa, S., 2002. Transverse migration of single bubbles in simple shear flows. Chem. Eng. Sci. 57, 1849.

Tsuchiya, K., Furumoto, A., Fang, L.-S., Zhang, J., 1997. Suspension viscosity and bubble size velocity in liquid–solid fluidized beds. Chem. Eng. Sci. 52, 3053.